Communications in Physics, Vol. 33, No. 2 (2023), pp. 111-122
DOI: https://doi.org/10.15625/0868-3166/17457

Regulation of continuum harmonic generation by using near-infrared chirped pulses

Cam-Tu Le[1,2,†], **Ngoc-Loan Phan**[3], **DinhDuy Vu**[3], **Cong Ngo**[3,4] **and Van-Hoang Le**[3,‡]

[1]*Atomic Molecular and Optical Physics Research Group, Advanced Institute of Materials Science, Ton Duc Thang University, Ho Chi Minh City, Vietnam*

[2]*Faculty of Applied Sciences, Ton Duc Thang University, Ho Chi Minh City, Vietnam*
19 Nguyen Huu Tho Street, Tan Phong Ward, District 7, Ho Chi Minh City, Vietnam

[3]*Computational Physics Key Laboratory, Department of Physics, Ho Chi Minh City University of Education, 280 An Duong Vuong Street, Ward 4, District 5, Ho Chi Minh City, Vietnam*

[4]*Department of Physics, Paderborn University, Warburger Strasse 100, D-33098 Paderborn, Germany*

E-mail: [†]lethicamtu@tdtu.edu.vn; [‡]hoanglv@hcmue.edu.vn

Received 24 August 2022; *Accepted for publication 26 October 2022*; *Published 31 March 2023*

Abstract. *It has been known that the broadband of continuum harmonics, a regular periodicity or a wide smooth range, is essential for generating attosecond pulses. However, the high-order rescatterings of electrons (HOR) can significantly affect this important part of high-order harmonic spectra. In the present work, we apply the method suggested in our previous studies to limit the HOR effect on the continuum harmonics by using up-chirped pulses with frequency increasing in time to regulate the high-order harmonic generation of an asymmetric molecule such as CO subjected to a near-infrared laser. To do so, we numerically calculate the high-order harmonic spectra using the time-dependent wave functions obtained within the framework of the single-active electron approximation. To analyze and regulate the HOR effect, we use the time-frequency analysis together with the kinetic energy maps obtained from the equation of electron motion in the laser electric field. These techniques reveal the high-order harmonic dynamics, especially the effect of chirped pulse on the manifestation of continuum harmonics. Based on this, we release the notice on choosing appropriate parameters to obtain the optimal continuum range of harmonics. Although the detailed analysis is given for the CO molecule, the method suggested is applicable for other polar molecules.*

Keywords: near-infrared chirped laser; multiple rescatterings; continuum harmonics; asymmetric molecules.

Classification numbers: 33.80.Eh.

1. Introduction

High-order harmonic generation (HHG) [1] is a nonlinear optical phenomenon with many important applications. Especially its underlying physics can be described by the three-step model [2, 3] by which an electron is detached from bound states to the continuum region, moves nearly free, acquires kinetic energy in the laser electric field, and then may recombine with the parent ion. In the final stage, the electron releases all accumulated energy as high-energy photons, so-called high-order harmonics. The fact that kinetic energy acquired by the electron is proportional to the laser parameters as $U_p \sim I\lambda^2$, where I and λ are the laser intensity and wavelength, suggests a possible way to extend the cutoff up to the keV region by utilizing the long wavelength of the laser. Consequently, attosecond or even zeptosecond pulses can be produced using near- or mid-infrared laser pulses [4]. However, when using such a longer wavelength laser, the electron can re-encounter many times before recombination, creating the sophisticated process due to the arising contribution of high-order rescatterings (HOR) into the harmonic spectrum [5–7]. In principle, to optimize the range of continuum harmonics whose benefit is producing attosecond pulse trains (APT), we should remove the contribution of HOR [6, 8].

Thanks to the development of laser technology, to fulfill the mentioned-above issues, we can either add an extra field, such as static [9] or vacuum ultraviolet (VUV) [6, 10], or use a specific laser with the frequency changing in time, i.e., the chirping form used in Ref. [11] as we figured out in our previous work [8]. In that study, we presented a specific case of an up-chirped laser with the frequencies increasing with time to demonstrate the possibility of controlling the HOR. However, we only briefly discussed how the appropriate value of chirp parameters could be chosen. Therefore, the object of the present paper is to show in detail the effect of the up-chirped laser on the formation of continuum harmonics of molecule CO and how to optimize these chirping parameters. We will show the detailed procedure consisting of two steps. The first is to obtain the dependence of the kinetic energy on the chirping parameters based on the classical electron trajectories [2], which may guide us in choosing the range of the optimal parameters. The second is to verify the prediction by examining the "actual" process of CO based on the HHG spectra calculated with the time-dependent wave functions within the single-active electron (SAE) approximation. It is worth mentioning that within this framework, we take dynamic core-electron polarization (DCEP) into account because of its important role in strong-field processes not only for polar molecules such as CO [12–17], OCS [18] but also for non-polar molecules such as CO_2 [19] and even for atoms such as Ca [20].

The rest of the paper is organized as follows. In Sec. 2, we briefly present the method of solving the time-dependent Schrödinger equation (TDSE) and calculating an HHG spectrum. Then, we describe the analysis method based on the time-frequency profile and classical kinetic energy. Section 3 devotes to our results and discussions. We finish the paper with the conclusion in Sec. 4.

2. Theoretical methods

2.1. Numerical method of calculating high-order harmonic spectra

In the HHG process, the electron wave packet is stretched by the laser electric field and consequently separated into bound and continuum parts resulting in an electric dipole. Because the laser field is periodical, the dipole is time-dependent that why the acceleration dipole

$\mathbf{a}(t) = \partial_t^2 \langle \Psi(\mathbf{r},t)|\mathbf{r}|\Psi(\mathbf{r},t)\rangle$ exists and causes the high-order harmonic generation. For a given frequency ω, the intensity of HHG emitted along the direction $\hat{e}$ can be obtained by the following formula [21]

$$S_{\hat{e}}(\omega) \propto |\hat{e}\cdot\mathbf{a}(\omega)|^2, \tag{1}$$

where $\mathbf{a}(\omega)$ is the Fourier transform of the time-dependent acceleration dipole of the electron as $\mathbf{a}(\omega) = \int \mathbf{a}(t)e^{i\omega t}\mathrm{d}t$. When taking the inverse Fourier transform of $\mathbf{a}(\omega)$ over a large range of harmonic orders $[\omega_i, \omega_f]$, especially a large range of continuum harmonics, we can attain the attosecond pulse trains as

$$I_{\mathrm{APT}}(t) = \left| \int_{\omega_i}^{\omega_f} \mathbf{a}(\omega)e^{i\omega t} d\omega \right|^2. \tag{2}$$

To calculate the HHG by formula (1), we use the electron wave function obtained by directly solving the time-dependent Schrödinger equation. Based on the assumption that only the active electron responses under subjection to the laser pulse, and to save the computational cost, we restrict the nuclei at the equilibrium position in the z axis and thereby construct the SAE potential $V_{\mathrm{SAE}}(\mathbf{r})$ for CO using the potential model approach [22]. The Schrödinger equation is then for one electron only. Its construction and the solving method were given in detail in our previous studies [8, 15]; therefore, we present here only the main points of the method.

The time-dependent Schrödinger equation describing the electronic wave function reads

$$i\frac{\partial}{\partial t}\Psi(\mathbf{r},t) = H(\mathbf{r},t)\Psi(\mathbf{r},t), \tag{3}$$

where $\Psi(\mathbf{r},t)$ is the active-electron wave function, and the Hamiltonian has the form $H(\mathbf{r},t) = -\nabla^2/2 + V_{\mathrm{SAE}}(\mathbf{r}) + \mathbf{E}(t)\cdot\mathbf{r} + V_{\mathrm{P}}(\mathbf{r},t)$. It should be noticed that for polar molecules such as CO, the polarization potential induced by the laser field is essential [12, 13] and is expressed as

$$V_{\mathrm{P}}(\mathbf{r},t) = -\frac{\hat{\alpha}_c\mathbf{E}(t)\cdot\mathbf{r}}{r^3}. \tag{4}$$

Here, $\hat{\alpha}_c$ is the core electrons' total polarizability, whose components are taken from Ref. [14]. The laser electric field $\mathbf{E}(t)$ is linearly polarized in the yz plane and makes an orientation angle θ with the molecular axis aligned along the z axis.

The temporal profile of the electric field for the chirped pulse is given as

$$E(t) = E_0 f(t)\sin(\omega_0 t + \delta(t) + \phi), \tag{5}$$

with E_0, ω_0, and $f(t)$ being respectively the laser pulse's peak amplitude, frequency, and envelope function. The phase between the envelope and the carrier wave is called the carrier-envelop phase, chosen in this work by $\phi = \pi/2$. The time-dependent term is $\delta(t) = -\beta_c \tanh[(t-t_0)/\tau_0]$ as given in Ref. [11], with β_c, τ_0, and t_0 being respectively the sweeping range, the steepness of the chirping function, and the position where the sweep is centered. With this, the change of these parameters can break the symmetry of the temporal profile of the laser pulse. To highlight the effect of the chirped laser on forming the continuum range obtained generally by few-cycle pulses, we use the multicycle laser, widely modeled by the trapezoidal envelope shape as

$$f(t) = \begin{cases} \frac{t}{t_{\mathrm{on}}} & \text{for } 0 \le t < t_{\mathrm{on}}, \\ 1, & \text{for } t_{\mathrm{on}} \le t \le t_{\mathrm{off}}, \\ -\frac{(t-\tau)}{(\tau - t_{\mathrm{off}})}, & \text{for } t_{\mathrm{off}} < t \le \tau \end{cases} \tag{6}$$

with τ being the pulse duration. Here, the turn-on and turn-off instants are defined by the equations $t_{\rm on} = n_{\rm on} T_0$ and $t_{\rm off} = (n_{\rm on} + n_c) T_0$ with $T_0 = 2\pi/\omega_0$ being the optical cycle of the driving pulse. The turn-on number and constant part are used in this work as $n_{\rm on} = 2$ and $n_c = 3$.

To solve the time-dependent Schrödinger equation (3), we expand the electronic wave function as a linear combination of eigenfunctions $\Phi_n^m(\mathbf{r})$ of the field-free Hamiltonian $H_0(\mathbf{r}) = -\nabla^2/2 + V_{\rm SAE}(\mathbf{r})$ as

$$\Psi(\mathbf{r},t) = \sum_{m=-\infty}^{+\infty} \sum_{n=1}^{+\infty} C_n^m(t) \Phi_n^m(\mathbf{r}). \tag{7}$$

In turn, the wave functions $\Phi_n^m(\mathbf{r})$ are expanded in terms of the B-spline functions [23] and the spherical harmonics. Plugging the wave function (7) into the time-dependent Schrödinger equation (3), we obtain equations for the time-dependent coefficients $C_n^m(t)$ which can be resolved by the forth-order Runge-Kutta method [15]. The solving procedure and the simulation parameters can be found in detail in Refs. [8, 15].

2.2. Time-frequency analysis

The calculated high-order harmonic spectra only give us the harmonic intensity at a given frequency ω but not the information of the instants when the harmonics are emitted. Therefore, we can not analyze the electron dynamics contributed to the HHG based only on the harmonics spectra. Nevertheless, a time-frequency map can be retrieved using the synchrosqueezed transform (SST) of the acceleration dipole [24] as

$$S(t,\Omega) = \int V(t,\eta) \frac{1}{\epsilon} h\left(\frac{\left|\Omega - \omega_f(t,\eta)\right|}{\epsilon} \right) \mathrm{d}\eta, \tag{8}$$

where $\epsilon > 0$ and small enough ($\epsilon = 0.05$ in this study), η is a positive real variable, $V(t,\eta)$ is a window function of the acceleration dipole in the time domain, for which there are several options to choose. In the present study, as in the previous, we use the Gabor transform [25, 26]

$$V(t,\eta) = \int \frac{1}{\sqrt{2\pi}\sigma} e^{-\frac{(t'-t)^2}{2\sigma^2}} a(t') e^{-i\eta(t'-t)} dt', \tag{9}$$

with $\sigma = (3\omega_0)^{-1}$ and $h(x) = e^{-x^2}/\sqrt{\pi}$. Also, the instantaneous frequency function $\omega_f(t,\eta)$ in Eq. (8) is given as

$$\omega_f(t,\eta) = \begin{cases} -\frac{i\partial_t V(t,\eta)}{V(t,\eta)}, & \text{if } V(t,\eta) \neq 0, \\ \infty, & \text{if } V(t,\eta) = 0. \end{cases} \tag{10}$$

2.3. Simulation of classical electron motion

To classify the electron trajectories into the order of rescattering, we need information about the ionization and recombination instants: t_i and t_r. For this purpose, we simulate the classical electron trajectories following the approach proposed in the work [2]; thereby, the kinetic energy of a returning electron is obtained by solving the one-dimensional classical equation of motion with the assumption that the electron sets free at t_i at the origin $z(t_i) = 0$ with initial velocity $\dot{z}(t_i) = 0$.

The recombination instant t_r can be estimated by finding the solutions of equation $z(t) = 0$. As a result, the kinetic energy at the moment of recombination $E_k = \frac{1}{2}\dot{z}^2(t_r)$ for every pair of instants (t_i, t_r) can determine the kinetic energy map. We note that there are several trajectories with

the same E_k, classified as long and short trajectories corresponding to different pairs of instants (t_i, t_r). Besides, the equation $z(t) = 0$ can have multiple solutions labeled by increasing order corresponding to the order of electron return, i.e., the first-, second-, ..., and so on. From the second-order to higher-order returns, one usually calls them as high-order returns.

The time-frequency analysis given in Subsec. *2.2*, together with the kinetic energy map obtained by classical simulation mentioned above, can reveal which electron returns contributed to each harmonic order that helps us analyze the effect of HOR on the continuum harmonics. We notice that there are some models in which the initial conditions of the electron are sampled randomly or generated as a distribution such as the classical trajectories Monte Carlo [27, 28] for a better quantitative description. However, in this work, the kinetic energy maps from the conventional model [2] are suitable for our purpose.

3. Results and discussions

In this section, we consider the harmonic spectra emitted from the CO molecules subjected to the near-infrared multicycle chirped pulses with wavelength of 1200 nm corresponding to $\omega_0 = 0.038$ a.u., the pulse duration $\tau = 7T_0 \approx 28$ fs, and the laser pulse's peak amplitude $E_0 = 0.05$ a.u. corresponding to intensity of 0.88×10^{14} W/cm^2. As mentioned above, the chirped pulse is characterized by the time-dependent chirping function

$$\delta(t) = -\beta_c \tanh[(t - t_0)/\tau_0]$$

with the parameters: β_c - the sweeping range, τ_0 - the steepness, and t_0 - the position where the sweep is centered. We aim to specify these chirping parameters to get the optimal continuum range of harmonics.

In the first step, we use the same parameters as in Ref. [11], where $\beta_c = 6.25$, $\tau_0 = 200$ a.u., and $t_0 = \tau_0/7$, to get the general picture of the chirping effect on the multiple rescatterings. As a result, the laser profile and the classical energy maps of the first-order returns of an electron moving in the chirped pulse are shown in Fig. 1. We can see that the difference between results for the chirp-free and chirped pulses only occurs in the first three optical cycles, i.e., at the ionization instants I_1, I_2, I_3 and at the corresponding recombination instants R_1, R_2, R_3 denoted in Fig. 1(b). We can also see in Fig. 1(b) that the excursion time of the electron in the chirped pulse (in the first three cycles) is greater than that in the chirp-free case (in the remaining cycles).

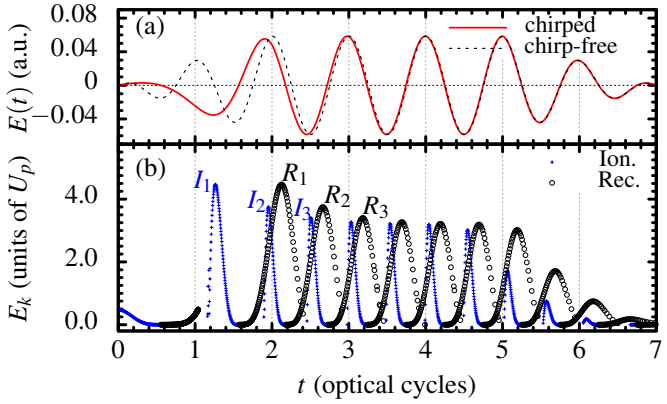

Fig. 1. (a) Temporal profile of the chirped pulse and (b) the classical kinetic energy of the first-order returns as a function of ionization (blue asterisks) and recombination instants (open black circles). For the sake of comparison, in panel (a), the laser with chirp-free is also plotted by the dotted black line.

Because of this, the figure shows greater kinetic energies at R_1, R_2, R_3. This circumstance means that the chirped pulse indeed can extend the cutoff in HHG spectra. However, we need further additional analysis to know its effect on the continuum harmonics. Here, the electron excursion time means the time interval between ionization and recombination events shown in Fig. 1(b).

From the above results, we have three electron trajectories corresponding to three pairs of instants: (I_1, R_1), (I_2, R_2), and (I_3, R_3), which have the greater kinetic energies at the recombination instants. To realize the contribution of these electron trajectories to the high-order harmonic generation, we show the high harmonic spectrum and its time-frequency profile for CO molecules in the chirped laser pulse in Fig. 2, presented for two opposite orientation angles, $\theta = 0^\circ$ and $\theta = 180^\circ$.

Two essential facts in Fig. 2 help us further define the continuum harmonics range from the time-frequency map. The first is the extension of the cutoff due to the chirping effect. Indeed, the cutoff is extended to the 67th-order at orientation $\theta = 0^\circ$ [Fig. 2(a)] and the 73rd-order at $\theta = 180^\circ$ [Fig. 2(b)]. These cutoffs corresponding to the laws $I_p + 3.42U_p$ and $I_p + 3.81U_p$ agree with the classical kinetic energies at R_3 and R_2, as shown in Fig. 1(b). This cutoff extension can be understood from the SST map in Fig. 2, which shows that the cutoff of the 67th-order in Fig. 2(a) is from electron return at the point R_3 (with highest intensity[1]), while the cutoff of the 73rd-order in Fig. 2(b) is from the point R_2 (with highest intensity[1]). Therefore, we conclude that the cutoff extension originates from the slight change in the chirped pulse's temporal profile, which raises a considerable difference in the kinetic energy of returning electron. This conclusion suggests a way to extend the cutoff by varying the chirped pulse parameters.

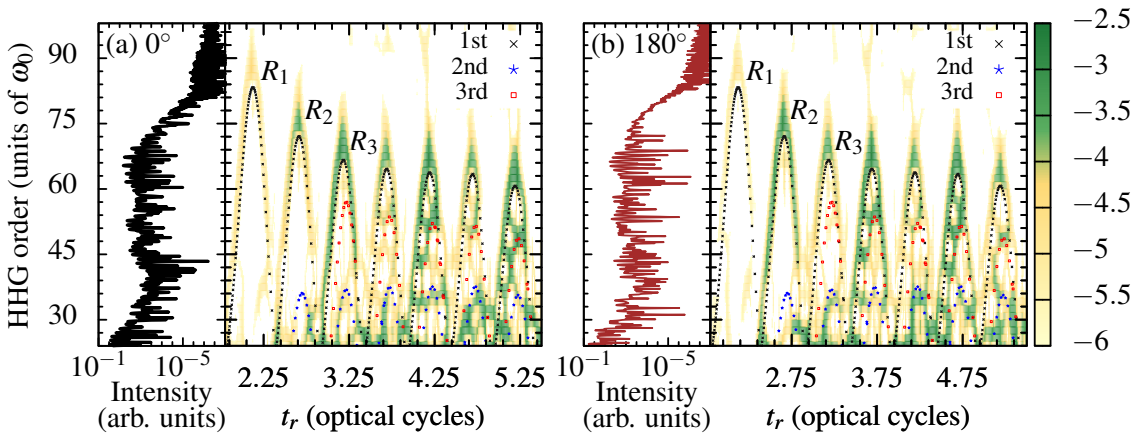

Fig. 2. Harmonic spectra and time-frequency profiles for the CO molecule subjected to the chirped laser pulse shown in Fig. 1(a) with two orientations 0° (a) and 180° (b). For the sake of comparison, the first-order, second-order and third-order returns of the classical kinetic energy maps are also superimposed.

The second fact is the different cutoffs for the two opposite orientations. This distinction originates from the asymmetry nature of the polar molecules and the symmetry-breaking of the temporal profile of chirped pulse [8]. Indeed, at orientation $\theta = 0^\circ$, the bursts around the odd

[1] the highest among three bursts R_1, R_2, R_3

points: R_3 ($t_r = 3.2T_0$), R_5 ($t_r = 4.2T_0$), R_7 ($t_r = 5.2T_0$) predominate, while at orientation $\theta = 180^\circ$, the bursts around even points R_2 ($t_r = 2.65T_0$), R_4 ($t_r = 3.7T_0$), R_6 ($t_r = 4.7T_0$) take over as shown in the SST spectra in Fig. 2. Moreover, one can see from Fig. 2(b) for orientation $\theta = 180^\circ$ that the maximum harmonic orders from the second- and third-order returns are smaller than the second-highest photon energies of the enhanced first-order returns at the point R_3. Consequently, the continuum range is then defined by the highest and the second-highest photon energies, i.e., from point R_2 to point R_3, corresponding to the harmonics 67th to 73rd. All these points belong to the first-order returns, meaning the continuum harmonics are obtained by eliminating high-order rescatterings using the chirped pulse. It brings us to the next investigation, examining how the appropriate parameters of the chirped pulse can affect the formation of continuum ranges.

Table 1. Energy difference ΔE_k between the highest kinetic energy $E_{k\max}$ and the second-highest one of the returning electron with different chirping parameters. Units of ΔE_k and $E_{k\max}$ are of U_p.

t_0/τ_0	$\beta_c = 6$		$\beta_c = 8$		$\beta_c = 10$		$\beta_c = 12$	
	$E_{k\max}$	ΔE_k	$E_{k\max}$	ΔE_k	$E_{k\max}$	ΔE_k	$E_{k\max}$	ΔE_k
0.1	4.21	0.50	5.54	1.17	5.64	1.69	4.75	1.06
0.2	4.58	0.73	4.75	1.06	6.99	2.81	5.39	1.57
0.3	5.15	1.11	5.33	1.50	4.51	0.87	6.52	2.51
0.4	6.08	1.78	6.25	2.24	4.99	1.24	9.21	**4.94**
0.5	7.87	**3.20**	7.99	**3.73**	5.79	1.87	4.65	0.98
0.6	5.20	1.37	7.38	2.76	7.32	**3.18**	5.22	1.42

We now go to the second step by changing chirped pulse parameters in the ranges: β_c from 6 to 12, and t_0 from $0.1\tau_0$ to $0.6\tau_0$, while τ_0 is kept to 200 a.u. as in Ref. [11] to get the optimal continuum harmonics range. Correspondingly, the temporal profile of the laser is modified, resulting in the change of the kinetic energy of returning electrons. With the guidance of classical prediction, we can narrow down considerably the cases of chirped pulse parameters needed for the quantum investigation. Indeed, we use the classical simulation for each set of the parameters to examine the difference between the highest and the second-highest kinetic energies of returning electrons, ΔE_k. The results are presented in Table 1 and demonstrated in Fig. 3 for clearer visualization. Here, differently from Refs. [11, 29], we are interested in the continuum range instead of the highest kinetic energy $E_{k\max}$ by themselves. Interestingly, Table 1 shows that the ΔE_k is maximum when E_k is also maximum for each given value of β_c. Particularly, with the variation of chirping parameters, the greatest value of ΔE_k is $4.94U_p$, corresponding to $E_{k\max} = 9.21U_p$ at $\beta_c = 12$ and $t_0 = 0.4\tau_0$.

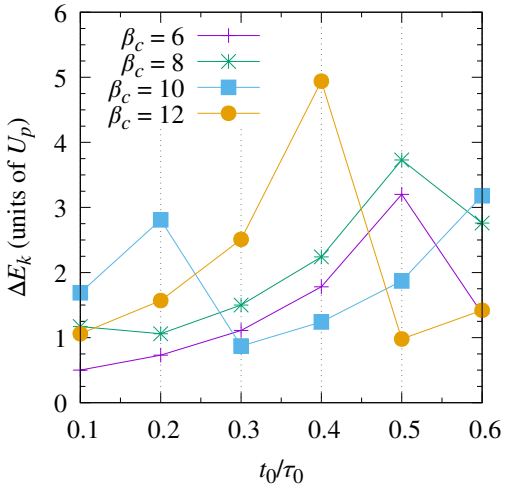

Fig. 3. Dependence of the energy difference between the highest and the second-highest kinetic energies of returning electron on the chirped pulse parameters β_c and t_0.

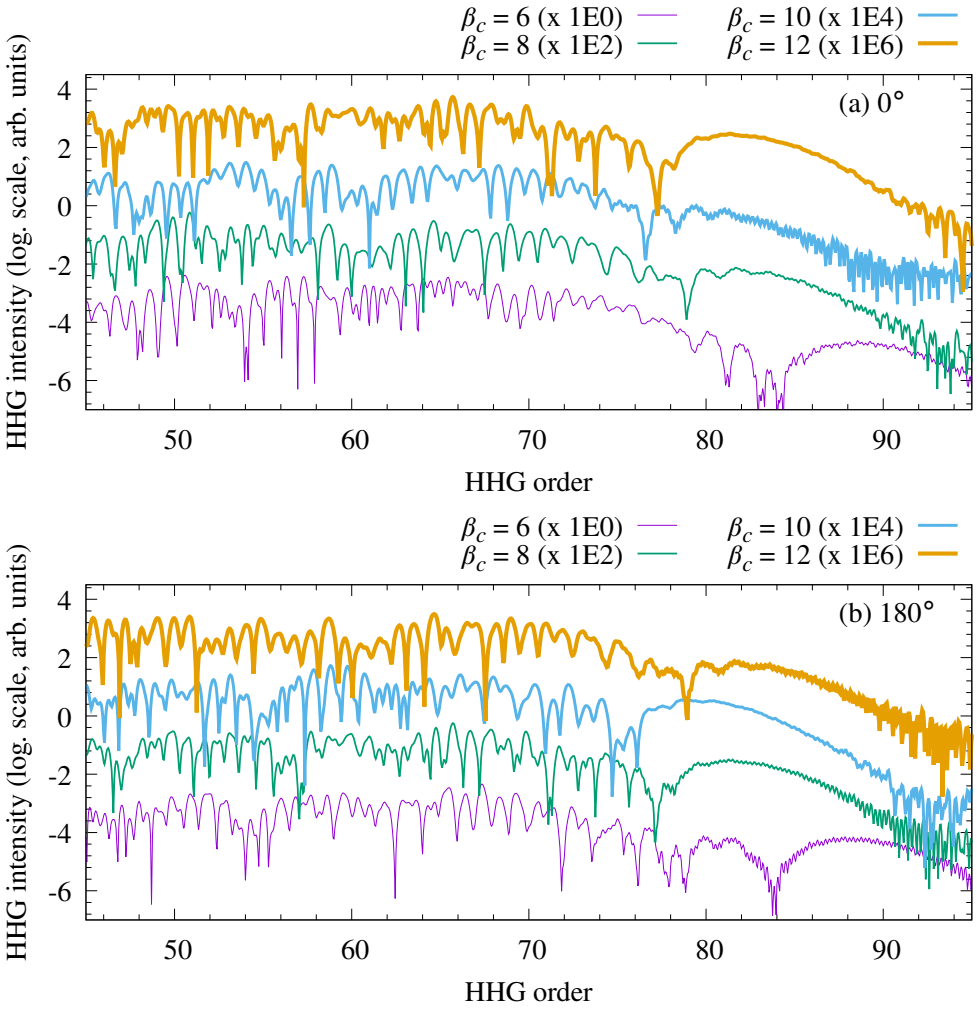

Fig. 4. HHG spectra at orientations $\theta = 0^{\circ}$ (a) and $\theta = 180^{\circ}$ (b) for the four sets of chirped pulse parameters which are bold in Table 1. For clarity, the spectra except for $\beta_c = 6$ and $t_0 = 0.5\tau_0$ are shifted vertically with factors shown in the legends.

Based on the classical results, we calculate harmonic spectra only for 4 cases of chirped pulse parameters indicated by bold numbers in Table 1. Obtained results are presented in Fig. 4. The HHG spectra for orientation $\theta = 0^{\circ}$ in Fig. 4(a) show that the greatest cutoff is at the 88th order, corresponding to $E_k = 4.77U_p$ and belonging to the parameters $\beta_c = 6, t_0 = 0.5\tau_0$. Interestingly, it is not the case of $E_{k\max} = 9.21U_p$ belonging to the parameters $\beta_c = 12, t_0 = 0.4\tau_0$ as predicted by the classical calculation. That is why we need the quantum calculation to justify the classical prediction. Furthermore, it is worth emphasizing that based on the classical calculation, this cutoff results from the recombination event at $t_r \approx 2.59T_0$ corresponding to the ionization instant $t_i \approx 1.78T_0$, not from $t_i \approx 0.52T_0$ which results in $E_{k\max} = 7.87U_p$. However, the continuum ranges for these cases are still quite short and just around the cutoff regions, with the greatest

bandwidth of about $1.0U_p$, i.e., from the harmonics 72 to 88. The generated pulses synthesized by Eq. (2) from these continuum ranges are presented in Fig. 5. The results show that except for $\beta_c = 12$ with the twin pulse, the generated pulses are a single pulse whose bandwidth and intensity are respectively shorter and higher with larger harmonic range. It has been known that in multicycle lasers, a train of twin pulses is generated from the long and short electron trajectories, while a train of single pulses indicates only one kind of electron trajectory existing [8]. Especially, these results show that the single attosecond pulse, usually achieved by few-cycle lasers, can be produced with multicycle pulses when using the chirping technique.

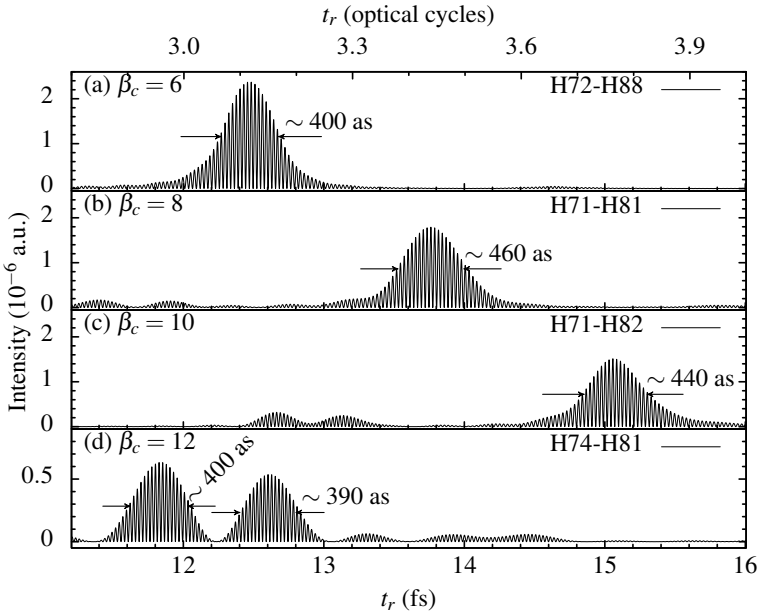

Fig. 5. Generated attosecond pulses obtained from the continuum regions of the HHG spectra of orientation $\theta = 0^\circ$ in Fig. 4(a).

Regarding the underlying mechanism of the single and twin pulse generation, it can be clearly explained by using the time-frequency profiles as in previous work [8]. Because the pattern of the time-frequency profiles for $\beta_c = 6, 8, 10$ is similar to Fig. 2, we can use it to explain the formation of the single pulses in Fig. 5. Indeed, for $\beta_c = 6, 8, 10$, the continuum range is also confined between R_2 and R_3. One can see that at $\theta = 0^\circ$, the continuum range is predominant by the highest orders of R_3 with only one kind of electron trajectory [see Fig. 2(a)], it leads to the generation of the single pulse. In the case of $\beta_c = 12$, because the laser's temporal profile is stretched very much, R_1 and R_2 are absent; thus, the continuum range is now confined between R_3 and the latter one. At $\theta = 0^\circ$, the continuum range is dominated by R_3, with both the long and short trajectories, it causes the generation of twin pulse.

For orientation $\theta = 180^\circ$, the results shown in Fig. 4(b) are the same. Due to the asymmetric characteristic of polar molecules, the harmonic structure, especially the harmonic resolution [8, 30] for the opposite direction, is quite different, as shown in Fig. 4(b). The resolution difference is due to the difference in the number of interference bursts, as figured out

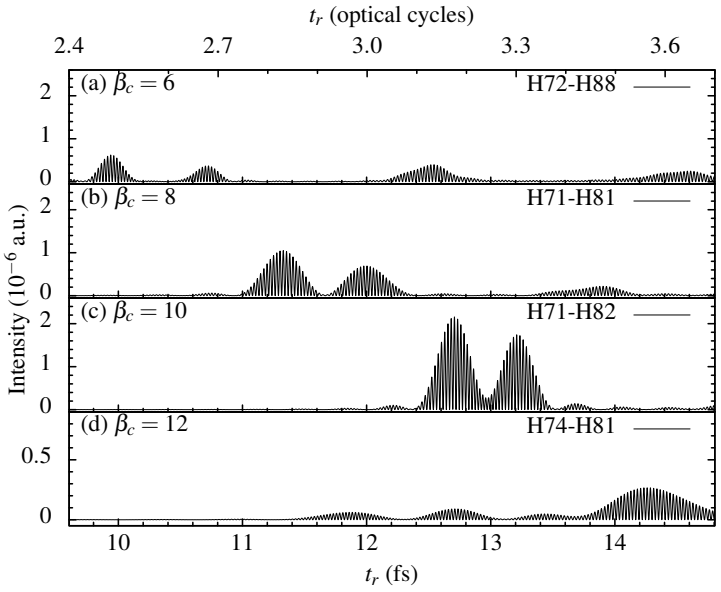

Fig. 6. -1cm Generated attosecond pulses obtained from the continuum regions of the HHG spectra of orientation $\theta = 180^\circ$ in Fig. 4(b).

in our previous study by analyzing the SST spectra [8]. In this work, we use another way to show this origin by using the temporal profile of the generated pulses exhibited in Fig. 6. As expected, in contrast to the case of orientation $\theta = 0^\circ$, the temporal profiles except for $\beta_c = 12$ are the twin pulses. Except for $\beta_c = 10$, the intensity of the generated pulses is lower than that of orientation $\theta = 0^\circ$. Moreover, the intensity of the generated pulses at $\theta = 180^\circ$ also changes vs. β_c more significantly than that of $\theta = 0^\circ$. The reason lies on the fact that the synthesized pulse of $\theta = 180^\circ$ is mainly determined by R_2 [as demonstrated in Fig. 2(b)], which correlates strongly to the ionization events in the turn-on phase of the laser. Additionally, the chirping effect also applies in this stage. Meanwhile, at $\theta = 0^\circ$, the role is taken over by R_3 correlating to instants that are less affected by the chirping effect. Therefore, the intensity of $\theta = 180^\circ$ is more sensitive to β_c than that of $\theta = 0^\circ$. These analyses suggest that the orientation of the molecular sample is essential to achieving the high efficiency of harmonic generation.

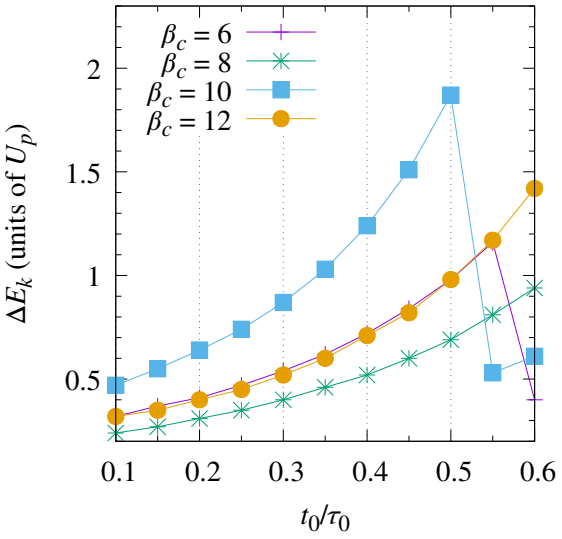

Fig. 7. Same as Fig. 3 but ignoring $t_i < 1.75T_0$.

Up to now, we focus only on the frequency of the continuum range but not on its intensity. In fact, with the careful investigation of the other cases, we realize that although the ionization with $t_i < 1.75T_0$ gives harmonics with high energy (around the cutoff), the ionization rate is very low. The reason is that ionization events occur in the turned-on phase of the pulse. Therefore, to improve the intensity of the continuum range, we should skim these instants. When considering $t_i > 1.75T_0$, the energy difference ΔE_k in Fig. 3 shows that the optimal values are $\beta_c = 10$ and $t_0 = 0.5\tau_0$, as found in Ref. [8].

4. Conclusions

In this work, we have studied the generation of the continuum spectrum of a polar molecule CO in multicycle near-infrared laser pulses and used the chirped field to eliminate the high-order rescattering effect on the continuum range. The high-order harmonic spectra are calculated numerically within the single-active electron approximation.

First, we pick a specific value of chirped pulse and analyze the underlying physics using the time-frequency analysis and the concept of electron trajectories. The results figure out that with such up-chirped pulses, the high-order returns do not perturb the continuum region of the high-order harmonic spectrum. Also, the slight change in the chirped pulse parameters can lead to a significant cutoff extension.

Then, we narrow down the range of chirping parameters to get the optimal continuum range by using the estimation from the classical simulation and then justify it by numerically solving the time-dependent Schrödinger equation. We notice that if also interested in the high-order harmonic generation efficiency, one should ignore the cases in which the highest high-order harmonic energy results from the ionization instants in the turned-on part of the laser pulse.

Conflict of interest

The authors have no conflict of interest to declare.

Acknowledgment

We are funded by Vietnam National Foundation for Science and Technology Development (NAFOSTED) under Grant No. 103.01-2020.57. The calculations were executed by the high performance computing cluster at Ho Chi Minh City University of Education, Vietnam.

References

[1] A. McPherson, G. Gibson, H. Jara, U. Johann, T. S. Luk, I. A. McIntyre et al., *Studies of multiphoton production of vacuum-ultraviolet radiation in the rare gases*, J. Opt. Soc. Am. B **4** (1987) 595.

[2] P. B. Corkum, *Plasma perspective on strong field multiphoton ionization*, Phys. Rev. Lett. **71** (1993) 1994.

[3] M. Lewenstein, P. Balcou, M. Y. Ivanov, A. L'Huillier and P. B. Corkum, *Theory of high-harmonic generation by low-frequency laser fields*, Phys. Rev. A **49** (1994) 2117.

[4] C. Hernández-García, J. A. Perez-Hernandez, T. Popmintchev, M. M. Murnane, H. C. Kapteyn, A. Jaron-Becker et al., *Zeptosecond high harmonic keV x-ray waveforms driven by midinfrared laser pulses*, Phys. Rev. Lett. **111** (2013) 033002.

[5] L. He, Y. Li, Z. Wang, Q. Zhang, P. Lan and P. Lu, *Quantum trajectories for high-order-harmonic generation from multiple rescattering events in the long-wavelength regime*, Phys. Rev. A **89** (2014) 053417.

[6] P.-C. Li, Y.-L. Sheu, H. Z. Jooya, X.-X. Zhou and S.-I. Chu, *Exploration of laser-driven electron-multirescattering dynamics in high-order harmonic generation*, Sci. Rep. **6** (2016) 32763.

[7] C.-P. Zhang, Y.-N. Pei, C.-L. Xia, X.-F. Jia and X.-Y. Miao, *Theoretical research on multiple rescatterings in the process of high-order harmonic generation from a helium atom with a long wavelength*, Laser Physics Letters **14** (2016) 015301.
[8] C.-T. Le, N.-L. Phan, D. D. Vu, C. Ngo and V.-H. Le, *Effect of multiple rescatterings on continuum harmonics from asymmetric molecules in multicycle lasers*, Phys. Chem. Chem. Phys. **24** (2022) 6053.
[9] W. Hong, P. Lu, W. Cao, P. Lan and X. Wang, *Control of quantum paths of high-order harmonics and attosecond pulse generation in the presence of a static electric field*, J. Phys. B: At. Mol. Opt. Phys. **40** (2007) 2321.
[10] M. R. Miller, C. Hernández-García, A. Jaroń Becker and A. Becker, *Targeting multiple rescatterings through vuv-controlled high-order-harmonic generation*, Phys. Rev. A **90** (2014) 053409.
[11] J. J. Carrera, X. M. Tong and S.-I. Chu, *Creation and control of a single coherent attosecond xuv pulse by few-cycle intense laser pulses*, Phys. Rev. A **74** (2006) 023404.
[12] B. Zhang, J. Yuan and Z. Zhao, *Dynamic core polarization in strong-field ionization of CO molecules*, Phys. Rev. Lett. **111** (2013) 163001.
[13] B. Zhang, J. Yuan and Z. Zhao, *Dynamic orbitals in high-order harmonic generation from CO molecules*, Phys. Rev. A **90** (2014) 035402.
[14] V.-H. Hoang, S.-F. Zhao, V.-H. Le and A.-T. Le, *Influence of permanent dipole and dynamic core-electron polarization on tunneling ionization of polar molecules*, Phys. Rev. A **95** (2017) 023407.
[15] C.-T. Le, V.-H. Hoang, L.-P. Tran and V.-H. Le, *Effect of the dynamic core-electron polarization of CO molecules on high-order harmonic generation*, Phys. Rev. A **97** (2018) 043405.
[16] M. Abu-samha and L. B. Madsen, *Effect of multielectron polarization in the strong-field ionization of the oriented CO molecule*, Phys. Rev. A **101** (2020) 013433.
[17] H. T. Nguyen, K.-N. H. Nguyen, N.-L. Phan, C.-T. Le, D. Vu, L.-P. Tran et al., *Imprints of multielectron polarization effects in odd-even harmonic generation from co molecules*, Phys. Rev. A **105** (2022) 023106.
[18] M. Abu-samha and L. B. Madsen, *Multielectron effects in strong-field ionization of the oriented ocs molecule*, Phys. Rev. A **102** (2020) 063111.
[19] C.-T. Le, D.-D. Vu, C. Ngo and V.-H. Le, *Influence of dynamic core-electron polarization on the structural minimum in high-order harmonics of CO_2 molecules*, Phys. Rev. A **100** (2019) 053418.
[20] Z. Zhao and J. Yuan, *Dynamical core polarization of two-active-electron systems in strong laser fields*, Phys. Rev. A **89** (2014) 023404.
[21] K. Burnett, V. C. Reed, J. Cooper and P. L. Knight, *Calculation of the background emitted during high-harmonic generation*, Phys. Rev. A **45** (1992) 3347.
[22] M. Abu-samha and L. B. Madsen, *Single-active-electron potentials for molecules in intense laser fields*, Phys. Rev. A **81** (2010) 033416.
[23] H. Bachau, E. Cormier, P. Decleva, J. E. Hansen and F. Martín, *Applications of B-splines in atomic and molecular physics*, Rep. Prog. Phys. **64** (2001) 1815.
[24] Y.-l. Sheu, L.-Y. Hsu, H.-t. Wu, P.-C. Li and S.-I. Chu, *A new time-frequency method to reveal quantum dynamics of atomic hydrogen in intense laser pulses: Synchrosqueezing transform*, AIP Advances **4** (2014) 117138.
[25] W. C. Lang and K. Forinash, *Time-frequency analysis with the continuous wavelet transform*, Am. J. Phys. **66** (1998) 794.
[26] C. C. Chirilă, I. Dreissigacker, E. V. van der Zwan and M. Lein, *Emission times in high-order harmonic generation*, Phys. Rev. A **81** (2010) 033412.
[27] J. Higuet, H. Ruf, N. Thiré, R. Cireasa, E. Constant, E. Cormier et al., *High-order harmonic spectroscopy of the cooper minimum in argon: Experimental and theoretical study*, Phys. Rev. A **83** (2011) 053401.
[28] Z. Shu, H. Liang, Y. Wang, S. Hu, S. Chen, H. Xu et al., *Channel coupling dynamics of deep-lying orbitals in molecular high-harmonic generation*, Phys. Rev. Lett. **128** (2022) 183202.
[29] Y. Xiang, Y. Niu and S. Gong, *Control of the high-order harmonics cutoff through the combination of a chirped laser and static electric field*, Phys. Rev. A **79** (2009) 053419.
[30] A. de Bohan, P. Antoine, D. B. Milošević and B. Piraux, *Phase-dependent harmonic emission with ultrashort laser pulses*, Phys. Rev. Lett. **81** (1998) 1837.